Hindawi
Journal of Engineering
Volume 2022, Article ID 3340489, 13 pages
https://doi.org/10.1155/2022/3340489

Research Article

Verification of a Torsional Behaviour Prediction Model for Reinforced Recycled Aggregate Concrete Beams

Aqeel H. Chkheiwer, Mazin A. Ahmed, and Zahir M. N. Hassan

Civil Department, Engineering College, University of Basrah, Basrah, Iraq

Correspondence should be addressed to Zahir M. N. Hassan; zahir.hassan@uobasrah.edu.iq

Received 14 June 2021; Revised 9 November 2021; Accepted 27 November 2021; Published 13 January 2022

Academic Editor: Y.A. Khulief

This study shows the torsional conduct of aggregate streaming beams of reinforced concrete recycling. Pure torsion was perceived for 15 reinforced concrete beams containing recycled concrete aggregates. The beams were grouped into five lengths and cross-sectional groups. The study's principal parameters were the various percentages of longitudinal steel reinforcement and the proportions of recycled aggregates. The beams were purely twisted until failure and investigated for torsional and crack behaviour. The findings show that the beams with maximum steel enhancement and standard aggregate exhibited maximum cracking power and ultimate torsional strength. Recycled aggregates increased the presence of splitting and the ultimate strength, and the effects of steel strengthening in recycled beams were apparent. In a second analysis, the whole torsional reaction of the beams was analytically predicted. A soft truss model was used and matched with test results for standard beams. A strong compromise was generally reached.

1. Introduction

Due to safety considerations and the renovation of old buildings, the use of horticulture in concrete production has increased over the past few years, with a consequence that the number of dilapidated materials has risen and that natural aggregates have been increasingly used, leading to a depletion of natural resources, which has required the use of recycled aggregates.

The softened membrane model (SMM) for predicting the behaviour of reinforced concrete (RC) membrane elements under shear was expanded by Chyuan-Hwan and Hsub [1] to predict the behaviour of RC members subjected to torsion. The softened membrane model for torsion (SMMT) is a new analytical method that accounts for the strain gradient of concrete struts in the shear flow zone by making two changes to the constitutive relationships of concrete. The SMMT may produce a reasonable forecast of torque-twist curves until reaching a peak, but it is not a decent simulation of postpeak curves according to Peng and Wong [2].

Chalioris [3] demonstrated that concrete confinement in RC members with close stirrup spacing has a significant impact on the torsional response. To explore the behaviour of torsional beams, a simple modification to the softened truss model to include the effect of confinement was also added. Chalioris [4] proposed an analytical approach for estimating the torsional capacity and overall behaviour of RC beams retrofitted with FRP textiles.

Chris and Karayannis [5, 6] discussed the construction of an analytical model for concrete element behaviour as torsion increases. For the behaviour of fracture process zones, the model relies on a specific numerical technique that uses constitutive relations defined in terms of normal stress and crack width. The construction of an effective model for concrete torsional analysis using a particular numerical technique that is correctly tailored to accommodate the smeared crack approach was also given. The SMMT has been extended to hollow RC members, thus determining concrete constitutive relationships for thin and thick-walled hollow RC members and developing a unified SMMT theory for hollow and solid RC members [7]. Under

torsion, the usual behavioural curve of a reinforced concrete element with longitudinal bars and stirrups has two separate regions: an elastic section before the first cracking and the part following the first cracking. The different characteristics of the response in these regions reveal the different nature of the load resisting mechanism in each case.

A study by Chalioris [8] focused on a method that integrates two separate analytical models to predict complete torsional behaviour. A smeared crack analysis for plain concrete in torsion was utilized to estimate the elastic component until the initial cracking, while the softened truss model was used to describe the postcracking response. Karayannis and Chalioris [9] proposed a new approach in which a bilinear stress-strain relationship was used to predict the capacity of prestressed concrete beams under pure torsion and torsion combined with shear and flexure, with a postcracking tension softening branch for the concrete in tension and special failure criteria for biaxial stress states. Steel fibre beams had more distinct failure processes than concrete beams because the fibres hindered crack formation and propagation. Steel fibre reinforcing has the primary benefit of establishing a crack-control mechanism and providing pseudoductility in postcracking behaviour. Steel fibres frequently improve the first-crack strength as a secondary effect, which is more connected to the quantity of fibres than to the efficiency of the fibres. This increase in first-crack strength is insignificant for low-volume fibre content [10]. Deifalla et al. [11] offered two models in their initial study. The first model made use of multilinear regression to optimize the constants of existing formulations. A second model was based on amending the American Concrete Institute (ACI) design code for reinforced concrete (RC) members to account for the influence of steel fibres on the torsional capacity of SFRC beams.

Many studies have focused on the properties and structural behaviour of concrete made from recycled aggregates (RACs) as an alternative to natural aggregates [12–22]. However, there is an obvious lack of studies with respect to torsion that address the subject, particularly in mixtures with high performance due to this coarse aggregate and its sharp corners. The concrete blend is very absorbent and difficult to deal with, but the availability of superplasticizers means that the concrete flux has been generated without impacting the blending ratios and the water growth.

However, there is very little literature on RAC torsional efficiency under pure torsion. To include an experimental and theoretical model to estimate the torsional potential and deformation foundation for functional engineering RAC applications, experiments were conducted in this study to better understand the torsional performance of RAC members under pure torsion.

2. Significance of Research

The main objective of this investigation is to validate a rough aggregate projection model of the structural activity of beams cast with flowing concrete, with different ratios substituted for torsion. The inquiry consisted of casting and testing fifteen beams into an experimental component. The key factors are the recycled composite proportion and the longitudinal strengthening ratio. The second part of the study validated Hsu's softened truss model [23] for the recycled mixing of aggregates in the mixture. Furthermore, in this research, we developed the "softened membrane model for torsion (SMMT)" theory for predicting a torque twist curve, including precracking and postcracking, as well as posttorsion reactions to the torque beam with recycled concrete as a coarse aggregate flowing concrete, by adding a factor that changes the tensile strength [24].

3. Softened Membrane Model for Torsion (SMMT)

3.1. Equilibrium Equations. If an outer torque T is subjected to the RC prismatic part, an inner torque generated by the circulatory shear flow Q resists the exterior torque, as shown in Figure 1(a). The shear flow q fills to a thickness td with the shear area flow [25, 26]. Factor A is under shear stress in the shear flow region (Figure 1(b)). According to the SMM [23], the balance of this variable in the plane accepts three equations as follows.

$$\{\sigma_l \;\; \sigma_t \;\; \sigma_{lt}\}^T = [T(\alpha_2)]\{\sigma_2^c \;\; \sigma_1^c \;\; \tau_{21}^c\}^T + \{\rho_l f_l \;\; \rho_t f_t \;\; 0\}^T. \tag{1}$$

The transformation matrix $[T(\alpha_2)]$ is given by

$$[T(\alpha_2)] = \begin{bmatrix} C^2 & S^2 & 2SC \\ S^2 & C^2 & -2SC \\ -SC & SC & C^2 - S^2 \end{bmatrix}, \tag{2}$$

where $c = \cos(\alpha_2)$, $s = \sin(\alpha_2)$. Element A under pure shear in the case of pure torsion and normal stresses $\sigma_1 = \sigma_t = 0$ and $\sigma_2 = 45$. The equilibrium of the full cross-section can be described by the following equation.

$$T = 2A_0 q = 2A_0 t_d \tau_{lt}. \tag{3}$$

3.2. The Equations of Compatibility. Three equations [23] can satisfy the compatibility in the plane of shear element A (Figure 1(b)):τ_{lt}

$$\left\{\varepsilon_l \;\; \varepsilon_t \;\; \frac{\gamma_{lt}}{2}\right\}^T = [T(\alpha_2)]\left\{\varepsilon_2 \;\; \varepsilon_1 \;\; \frac{\gamma_{21}}{2}\right\}^T. \tag{4}$$

The equations (4) and (5) can be described as [15]

$$\theta = \frac{P_0}{2A_0}\gamma_{lt}, \tag{5}$$

$$\phi = \theta \sin 2\alpha_2. \tag{6}$$

The strain gradient is shown in Figure 2(a) in one and two directions by triangular strain diagrams. The distribution of the strain is believed to be linear according to rotating angle theory, and the diameter of the concrete stress area of the strut is assumed to be the width of the shear flux zone t_{d}, so

$$t_d = \frac{\overline{\varepsilon}_{2s}}{\phi}. \tag{7}$$

The smeared (or average) uniaxial strain ε_{2s} is assumed to be related to the maximum uniaxial strain ε_{2s} at the surface by $\varepsilon_2 = \varepsilon_{2s}/2$ [25].

Equation replacement and distortion. The following explicit expression is given in the computation equations of p_0 and A_0 rectangular parts, as described in the nomenclature, for the calculation of the effective thickness td of the shear flow field:

$$t_d = \frac{1}{2(Q+4)} \times \left[P_C\left(1+\frac{Q}{2}\right) - \sqrt{\left(1+\frac{Q}{2}\right)^2 P_C^2 - 4Q(Q+4)A_C} \right], \tag{8}$$

where

$$Q = \frac{2\overline{\varepsilon}_{2S}}{\gamma_{lt}\sin 2\alpha_2} = \frac{4\overline{\varepsilon}_2}{\gamma_{lt}\sin 2\alpha_2}. \tag{9}$$

3.3. The Relationships between Biaxial and Uniaxial Strains. The relationships are defined in algebraic equations by Hsu and Zhu [23]. However, the expressions in the matrix are

$$\left\{\overline{\varepsilon}_2, \overline{\varepsilon}_1, \frac{\gamma_{21}}{2}\right\}^T = [V]\left\{\varepsilon_2, \varepsilon_1, \frac{\gamma_{21}}{2}\right\}^T, \tag{10}$$

where $[V]$ is the conversion matrix:

$$[V] = \begin{bmatrix} \dfrac{1}{1-\nu_{12}\nu_{21}} & \dfrac{\nu_{21}}{1-\nu_{12}\nu_{21}} & 0 \\ \dfrac{\nu_{21}}{1-\nu_{12}\nu_{21}} & \dfrac{\nu_{21}}{1-\nu_{12}\nu_{21}} & 0 \\ 0 & 0 & 1 \end{bmatrix}, \tag{11}$$

$$\left\{\overline{\varepsilon}_l, \overline{\varepsilon}_t, \frac{\gamma_{lt}}{2}\right\}^T = \left[T(\alpha_2)\right]\left\{\overline{\varepsilon}_2, \overline{\varepsilon}_1, \frac{\gamma_{21}}{2}\right\}^T. \tag{12}$$

3.4. Constitutive Relationships of Concrete in Compression. As seen in the SMM [26], the relationship between the compressive stress and strain of soft cement is shown in Figure 3. The decrease in the compressive strength can be reflected in the coefficient of the reinforcement. Three factors illustrate this: the tensile tension in the principal direction, the angles of difference β, and the pressure of concrete $f-c$. To calculate the average compressive force for concrete struts, k_1 is used as the average torque stress factor for RA-STM.

$$\sigma_2^C = K_{1C}\xi f_c'. \tag{13}$$

The average stress factor k_{1c} is obtained by integrating the stress-strain equations as follows:

$$K_{1C} = \frac{\overline{\varepsilon}_{2S}}{\xi\varepsilon_0} - \frac{\left(\overline{\varepsilon}_{2S}\right)^2}{3\left(\xi\varepsilon_0\right)^2}, \quad \text{for } \frac{\overline{\varepsilon}_{2S}}{\xi\varepsilon_0} \le 1,$$
$$K_{1C} = 1 - \frac{\xi\varepsilon_0}{\overline{\varepsilon}_{2S}} - \frac{\left(\overline{\varepsilon}_{2S} - \xi\varepsilon_0\right)^3}{3\overline{\varepsilon}_{2S}\left(4\varepsilon_0 - \xi\varepsilon_0\right)^2}, \quad \text{for } \frac{\overline{\varepsilon}_{2S}}{\xi\varepsilon_0} > 1. \tag{14}$$

3.5. Constitutive Relationships of Concrete in Tension. The tensile tension of concrete is neglected for the theories of torsion [27–34]. None of these models predicts the cracking torque, *T*cr, or the torsional torsion response to precracking and prepeak rigidity. The latest SMMT effectively implements this impact to overcome these obstacles. The curvature ϕ in two directions is the second derivative of w with respect to the length in the 2 directions, which is related to the angle of twist θ and the fixed angle α_2 by equation (6). Similarly, in the single direction, we can derive the curvature:

$$\varphi = \frac{\mathrm{d}^2 w}{\mathrm{d}t^2} = -\theta\sin 2\alpha_2 = -\phi. \tag{15}$$

The maximum tensile strain ε_{1s} can be calculated as

$$\overline{\varepsilon}_{1S} = \varphi t_d,$$
$$\overline{\varepsilon}_1 = \frac{\overline{\varepsilon}_{1S}}{2}, \tag{16}$$

$$\sigma_1^C = K_{1t} f_{cr}, \tag{17}$$

$$K_{1t} = \frac{1}{\overline{\varepsilon}_{1S} f_{cr}} \int_0^{\overline{\varepsilon}_{1S}} \sigma_1\left(\overline{\varepsilon}_1\right)\mathrm{d}\overline{\varepsilon}_1, \tag{18}$$

where σ_1 (ε_1) is the uniaxial tensile stress-strain relationship of concrete.

$$K_{1t} = \frac{\overline{\varepsilon}_{1S}}{2\varepsilon_{cr}}, \quad \text{for } \frac{\overline{\varepsilon}_{1S}}{\varepsilon_{cr}} \le 1,$$
$$K_{1t} = \frac{\varepsilon_{cr}}{2\overline{\varepsilon}_{1S}} + \frac{\left(\varepsilon_{cr}\right)^{0.4}}{(0.6)\overline{\varepsilon}_{1S}}\left[\left(\overline{\varepsilon}_{1S}\right)^{0.6} - \left(\varepsilon_{cr}\right)^{0.6}\right], \quad \text{for } \frac{\overline{\varepsilon}_{1S}}{\varepsilon_{cr}} > 1. \tag{19}$$

3.6. Constitutive Relationships of Concrete in Shear. A companied representation of the rational shear modulus [32] in the SMM with the SMMT to relate the shear stress strain of concrete is as follows:

$$\tau_{21}^c = \frac{\sigma_1^c - \sigma_2^c}{2\left(\varepsilon_1 - \varepsilon_2\right)}\gamma_{21}. \tag{20}$$

3.7. Algorithm Solution. Figure 4 shows the algorithm solution for the proposed SMMT, which is an extension of the SMM solution. The first two basic equilibrium equations in equation (1) are described in the SMM and then summed and subtracted to obtain the two equations, which are used as the convergence criteria for the solution procedure [23]:

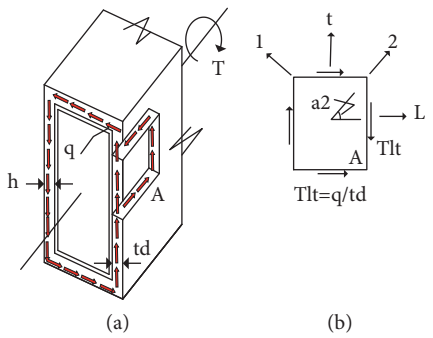

Figure 1: Reinforced concrete section subjected to torsion: (a) shear flow of the cross-section and (b) in-plane stress state of element A.

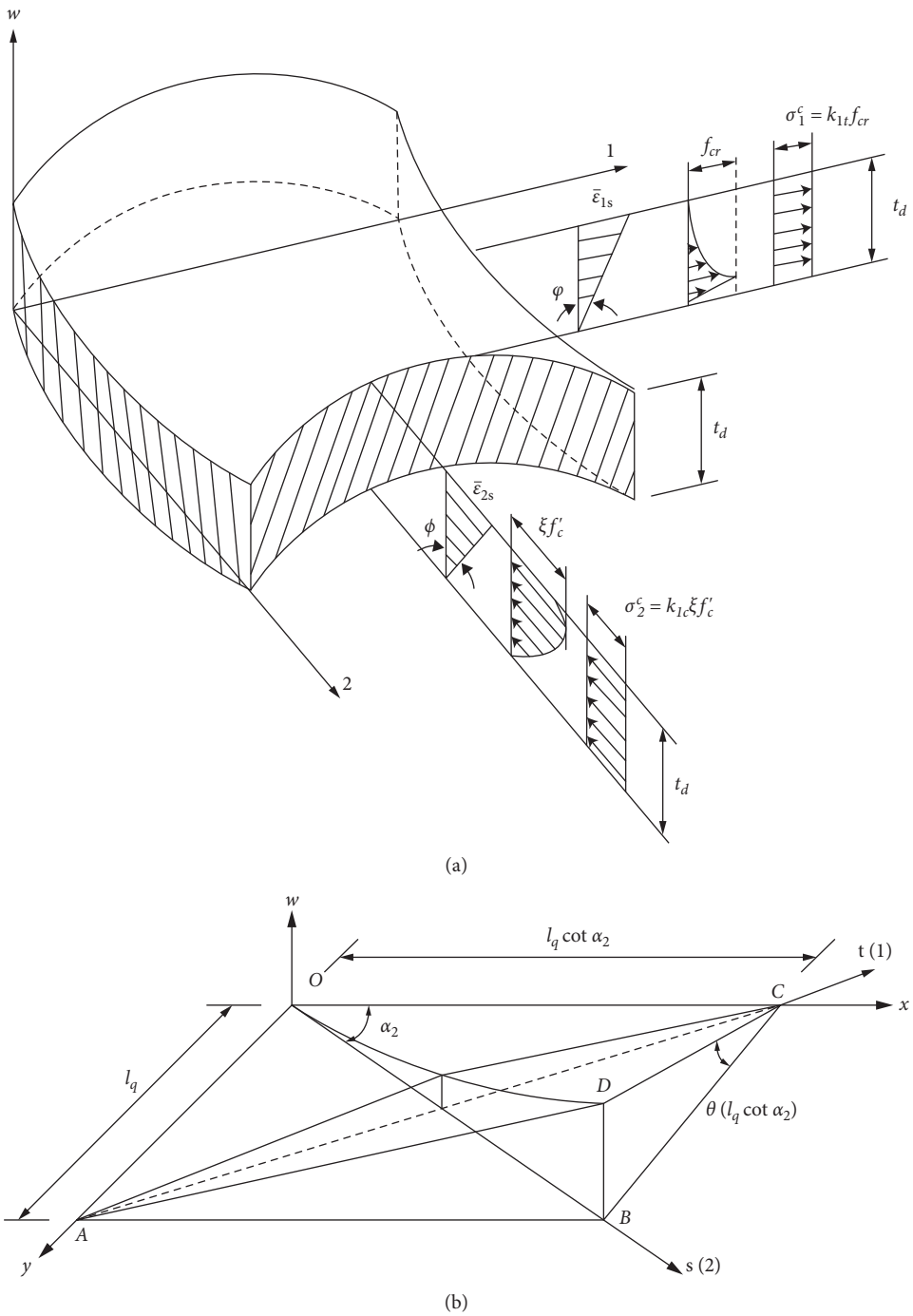

Figure 2: Concrete strut bending: (a) biaxial stress state without plane bending and (b) hyperbolic paraboloid surface for out-of-plane bending.

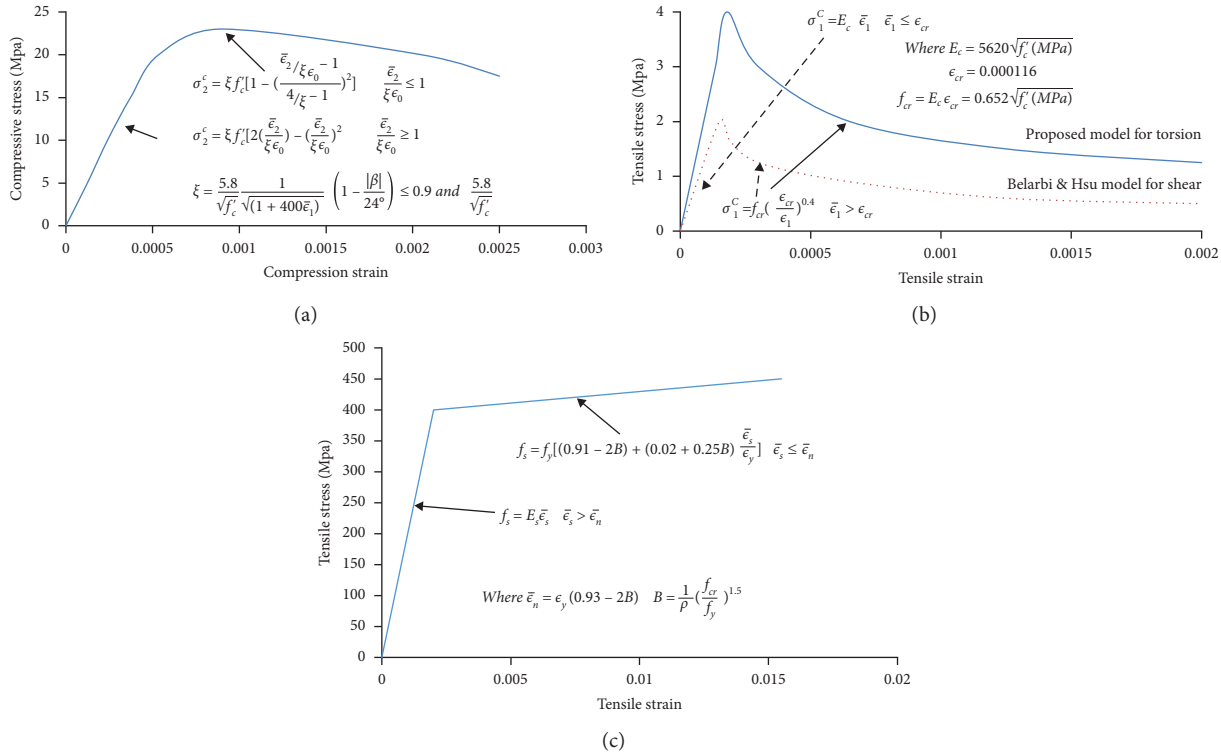

Figure 3: The constitutive relations: (a) concrete in compression, (b) concrete in tension, and (c) mild steel embedded in concrete.

$$\rho_l f_l + \rho_t f_t = (\sigma_l + \sigma_t) - (\sigma_2^c + \sigma_1^c), \tag{21}$$

$$\rho_l f_l - \rho_t f_t = (\sigma_l - \sigma_t) - (\sigma_2^c - \sigma_1^c)\cos 2\alpha_2 - 2\tau_{21}^c \sin 2\alpha_2. \tag{22}$$

Note that one of the differences between the algorithms of the SMMT and the SMM is the variable td (and so are the reinforcement ratios σ_1 and σ_t) in the SMMT.

4. Test Program

Fifteen beams were tested under pure torsion in an experimental program. The key variables were the longitudinal strengthening ratio (0.007 (8-5-010 mm), 0.01 (12 – μ10 mm) and recycled aggregate replacement ratio (16 – μ10 mm) (0, 25, 50, 75, and 100%). They are both 300 ∗ 300 mm and 1500 mm high, and each beam has an identical cross-section. For each beam, the transversal arming was the same and was 10 mm for 120 mm, as shown in Figure 5. Table 1 provides the details of the tested beams. The number after letter B shows the number of linear bars, and the proportion of substituted recycled aggregates is after the letter *R*.

This analysis used normal Portland cement, a raw and fine natural aggregate from Al-Zubair. The unit weights of the coarse and fine aggregates were 1630 and 1740 kg/m^3, and the water absorption was 0.67 and 1.2%, respectively. The recycled add-ons (with a compressive strength of 40 MPa) that were carried out for testing in the laboratory were derived from the demolition of concrete cubes and then graded to a maximum size of 19 mm for ASTM C33 [35] scoring. Fu and Tang [33] used a similar natural crushed gravel grading, but their water absorption and unit weight were 5.3% and 1253 kg/m^3, respectively. This means that there is a difference in unit weight and absorption between natural and recycled aggregates; therefore, all aggregates in the SSD condition have been used. For high workability, a high-performance superplasticizer with a specific gravity of 1.1 and a total solid content of 30% was used in all mixtures. The amount of superplasticizer was observed to increase as the percentage of recycled aggregate replacement increased, as given in Table 2. For blending, casting, and curing, regular tap water was used.

The concrete blend was intended to provide standard concrete with 32 MPa at 28 days of curing (0% recycled aggregates). They were produced at 1.0, 1.87, 2.69, and 0.41% (cement: gravel and water cement proportions, respectively). Four concrete mixtures, each with a different percentage of the total recycled concrete substitution of cough aggregates, were generated according to Table 2 (0, 25, 50, 75, and 100%). The renewable steel yield strength and elasticity modulus were 420 N/mm^2 and 2×10^5 N/mm^2, respectively.

For each group, the compressive strength of the concrete was determined using the average of three cylinders of 300 mm diameter and 3150 mm height based on ASTM C39 [36] and C496 [37]. This is the basis of the compression. Both specimens (beams and cylinders) were cast together and consciously protected for seven days with wet burlap and then held together in the laboratory until testing under the same atmospheric conditions (28 days). The calculated properties of the concrete mixtures are given in Table 2.

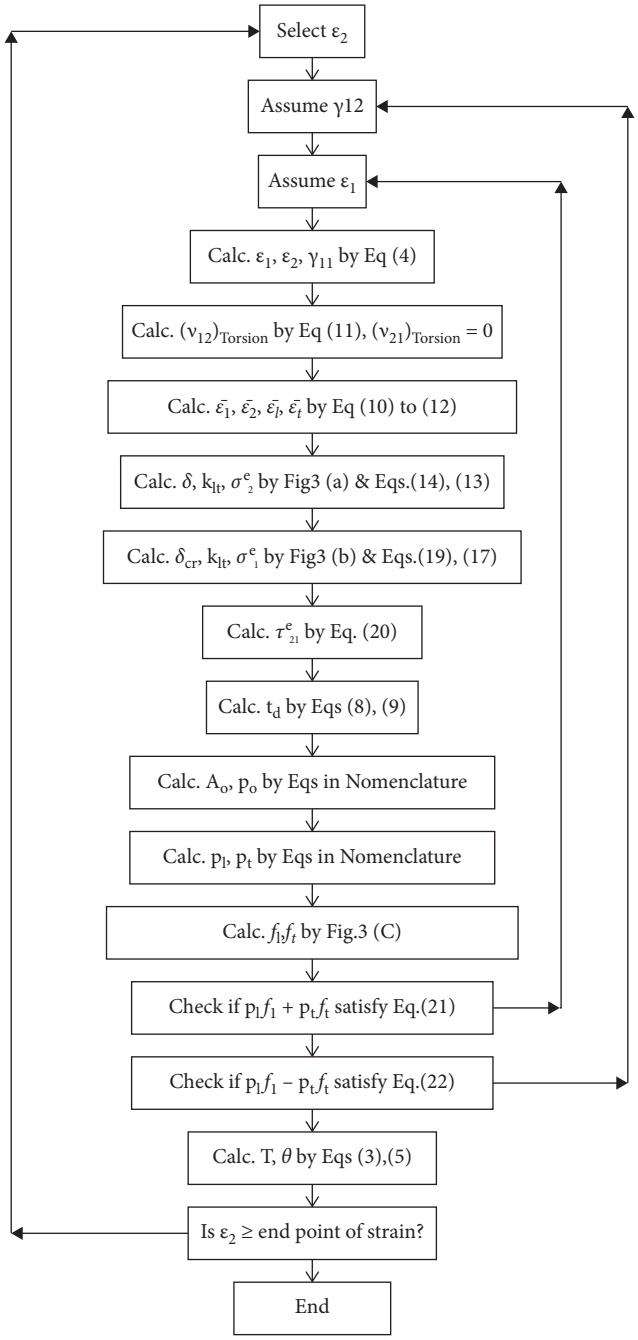

Figure 4: Solution algorithm for the SMMT.

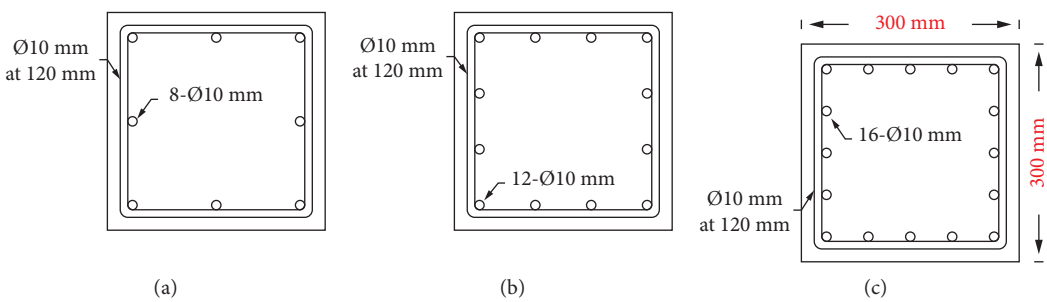

Figure 5: Reinforcement details of the tested beams. (a) $\rho = 0.007$. (b) $\rho = 0.01$. (c) $\rho = 0.014$.

Table 1: Details of the tested beams.

Group	Beam destination	Reinforcement ratio (ρ)	Recycled aggregate percentage (%)
A	B8R0	0.007	0
	B12R0	0.010	0
	B16R0	0.014	0
B	B8R25	0.007	25
	B12R25	0.010	25
	B16R25	0.014	25
C	B8R50	0.007	50
	B12R50	0.010	50
	B16R50	0.014	50
D	B8R75	0.007	75
	B12R75	0.010	75
	B16R75	0.014	75
E	B8R100	0.007	100
	B12R100	0.010	100
	B16R100	0.014	100

Table 2: Concrete mixture proportions and properties.

Ingredient	Unit	Recycled aggregate replacement (%)				
		0	25	50	75	100
Cement type I	kg/m^3	400	400	400	400	400
Fine aggregate	kg/m^3	748	748	748	748	748
Water	kg/m^3	176	176	176	176	176
Coarse aggregate	kg/m^3	1076	807	538	269	0
Recycled aggregate*	kg/m^3	0	207	413	620	828
Superplasticizer	kg/m^3	2.400	2.789	3.012	3.256	3.650
Properties						
Slump	mm	240	238	232	236	233
Compressive strength	MPa	33.3	30.6	28.9	26.5	24.6
Splitting tensile strength	MPa	2.85	2.53	2.13	2.05	1.88

Both beams were measured with a maximum capacity of 300 tons using a universal testing machine (Model 855, IMFI system), as shown in Figure 6. The clear beam span was 1.2 metres. The beams on free-assisted rollers were mounted on either end of the rig. A series of linear transduction transducers (LVDTs) was positioned under four branches that were projected normal to the beam axis (to quantify torsional rotations). The longitudinal strain was measured by three 10 mm long electrical resistance gauges attached to one of its edges at a space of 50 mm. The electric resistance strains of diagonal concrete strains were also tested. Three gauges with an inclination of 45° to the beam axis were placed on the centre beam. The registered numbers with their widths were determined with a precision of ±0.001 mm with a handheld microscope. Figure 6 shows the research configuration.

5. Experimental Results and Discussion

5.1. Behaviour of Beams under Loading. During the first loading stages, the checked beam was free of cracks at a slight twisting angle (AD) before its application hit the moment of torsional cracking (T_{cr}), which was the torque of a cracking process. At first, a crack appeared on the one side of the web, and after T_{cr} occurred, the applied torque increased significantly. Other cracks were created on the other side of the network to create a complete helical crack pattern. Both stretched upwards and downwards. However, the last torsional moment (T_u) reflects the load capacity.

5.2. Crack and Ultimate Torque. Table 3 provides the experimental results of the tested beams: cracking torque (T_{cr}), ultimate torque (T_u), and the angle of twisting of the beam. The relation between the ultimate load and recycled aggregate replacement ratio for different ratios of longitudinal reinforcement is shown in Figure 7.

The effect of recycled aggregate is clear when studying beams B8R0, B8R25, B8R50, B8R75, and B8R100, which have 0.007 reinforcement, and with different percentages of recycled aggregate 0, 25, 50, 75, and 100%, the crack torque and ultimate torque decrease with increases in recycled aggregate; this effect is largest for beams with 100% recycled aggregate. Additionally, the decreases in T_{cr} with an increase in recycled aggregate are greater than those in T_u.

The earlier result is the same for the beam community as for the strengthening increase from 0.010 to 0.014, however, with less impact on the beams B16R0, B16R25, B16R50, B16R75, and B16R100. This means that the recycled aggregate has a strong strengthening impact.

Table 3 provides that the ratio of ultimate (T_u) torque is 30% higher for beams in group E and 50% higher for

Figure 6: Test setup.

Table 3: Summary of test results.

Group	Beam destination	T_{cr} kN·m	T_u kN·m	(T_{cr}/T_{crcont})	(T_u/T_{ucont})	θ_{cr}	$(\theta_{cr}/\theta_{crcont})$	θ_u	$(\theta_u/\theta_{ucont})$
A	B8R0	103	110	—	—	1.20	—	2.06	—
	B12R0	87	130	0.84	1.18	1.04	0.87	2.54	1.23
	B16R0	128	156	1.24	1.40	0.75	0.63	3.65	1.77
B	B8R25	94	105	—	—	0.90	—	1.90	—
	B12R25	74	122	0.78	1.16	0.84	0.93	2.10	1.10
	B16R25	117	147	1.24	1.40	0.66	0.73	3.00	1.58
C	B8R50	88	97	—	—	0.70	—	1.30	—
	B12R50	74	117	1.20	1.20	0.67	0.96	1.10	0.85
	B16R50	133	141	1.51	1.45	0.51	0.73	2.10	1.61
D	B8R75	80	90	—	—	0.52	—	1.00	—
	B12R75	70	112	0.87	1.24	0.43	0.83	0.90	0.9
	B16R75	119	136	1.48	1.51	0.37	0.71	1.86	1.86
E	B8R100	69	75	—	—	0.39	—	0.77	—
	B12R100	62	97	0.90	1.30	0.30	0.77	0.86	1.12
	B16R100	108	114	1.57	1.52	0.27	0.69	1.33	1.73

B12R100 and B16R100 compared to B8R100, so the improvement of the ratio of strengthening leads to increased strength torque for beams. This also occurs in beams made with natural aggregate, the B8R0, B12R0, and B16R0 beams (group A), but they exhibit less increase in Tu than the beams in group E: 18% and 40% for beams B12R0 and B16R0 compared with B8R0, respectively. This is due to the effect of recycled aggregate, where its presence in the concrete mix increases the work of reinforcement.

5.3. Torque-Twisting Angle Curves. Figures 8 and 9 show the relationships between the torque applied for typically tested beams and the twist per unit volume. The statistics show that all beams are linear until cracking and more rigid if the percentage of strengthening is high ($\acute{c} = 0.014$); then, twist angles rise without an increase in torque caused by tension redistribution from concrete to refinement. The beam becomes nonlinear after this stage and before its end, with a decrease in torsional rigidity. After the cracking stage, the beam with a high reinforcement ratio demonstrated ductile performance. It should also be noted that the previous behaviour of recycled aggregates increased, but that the ductile behaviour was lower when using 100% recycled aggregates. The torsional angle values are given in Table 2 with critical load (move-cr) and ultimate load (move-u) per unit volume. Beam B16R0, which incorporates steel strengthening = −0.014, is efficient in height with standard aggregates. The maximum torque and twisting angle is 156 kNm and 3.65 deg/m, respectively. The lower performance is 75 kNm and 0.77 degree/m with a dwindling torque and angle, while the B8R100 beam is 0.007 and uses 100% recycled aggregate. The inclusion of the steel strengthening induces improved cracking torque as well as postcracking rigidity and torsional resistance from the load-response curves for beams B8R25, B12R25, and B16R25, which used a 25% recycled aggregation of 0.007, 0.010, and 0.014 reinforcement, respectively.

5.4. Mode of Failure. The standard failure of the test beams is shown in Figure 10. The standard aggregate beams tend to

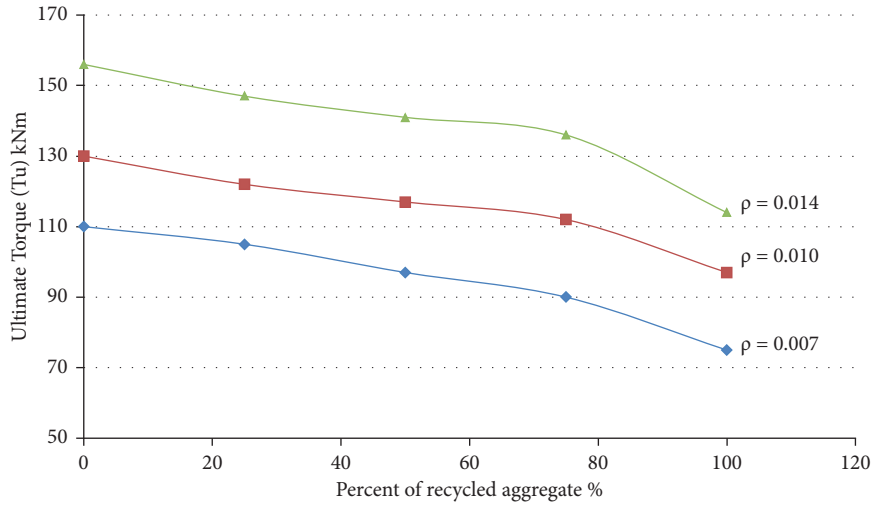

Figure 7: Relation between the ultimate load and the percent of recycled aggregate for different ratios of longitudinal reinforcement.

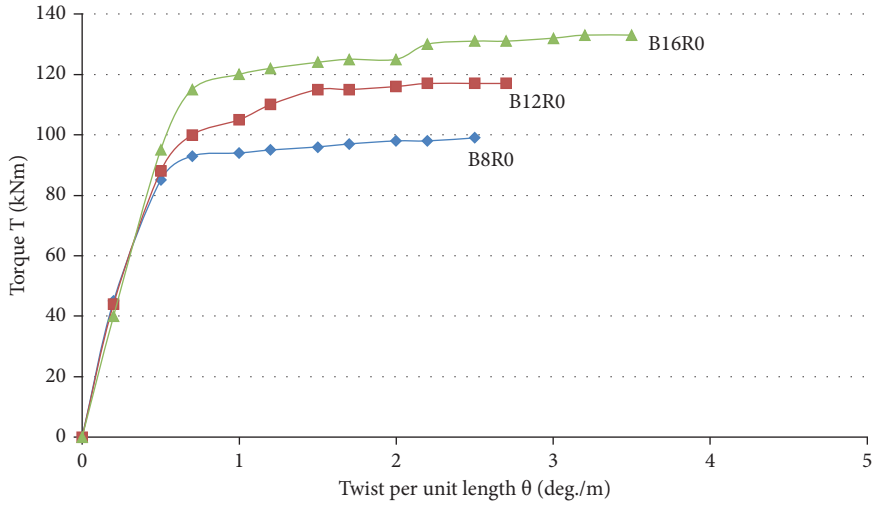

Figure 8: Experimental torque-twist response for beams with normal aggregate.

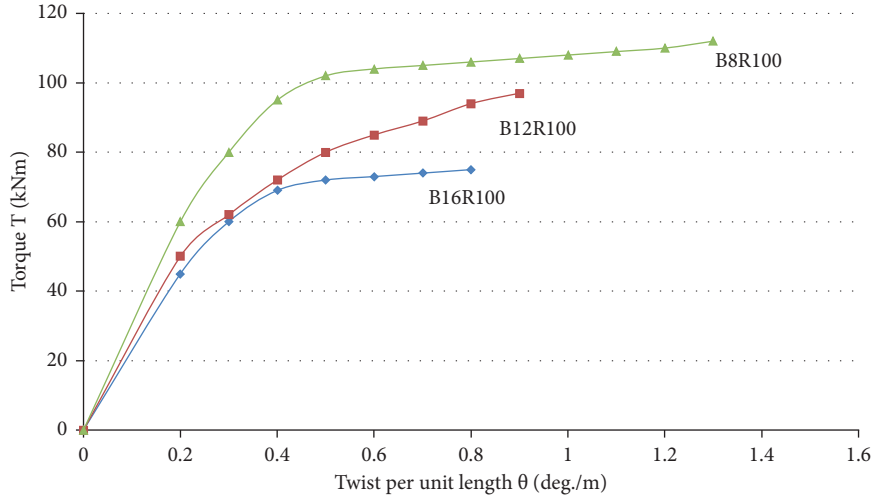

Figure 9: Experimental torque-twist response for beams with 100% recycled aggregate.

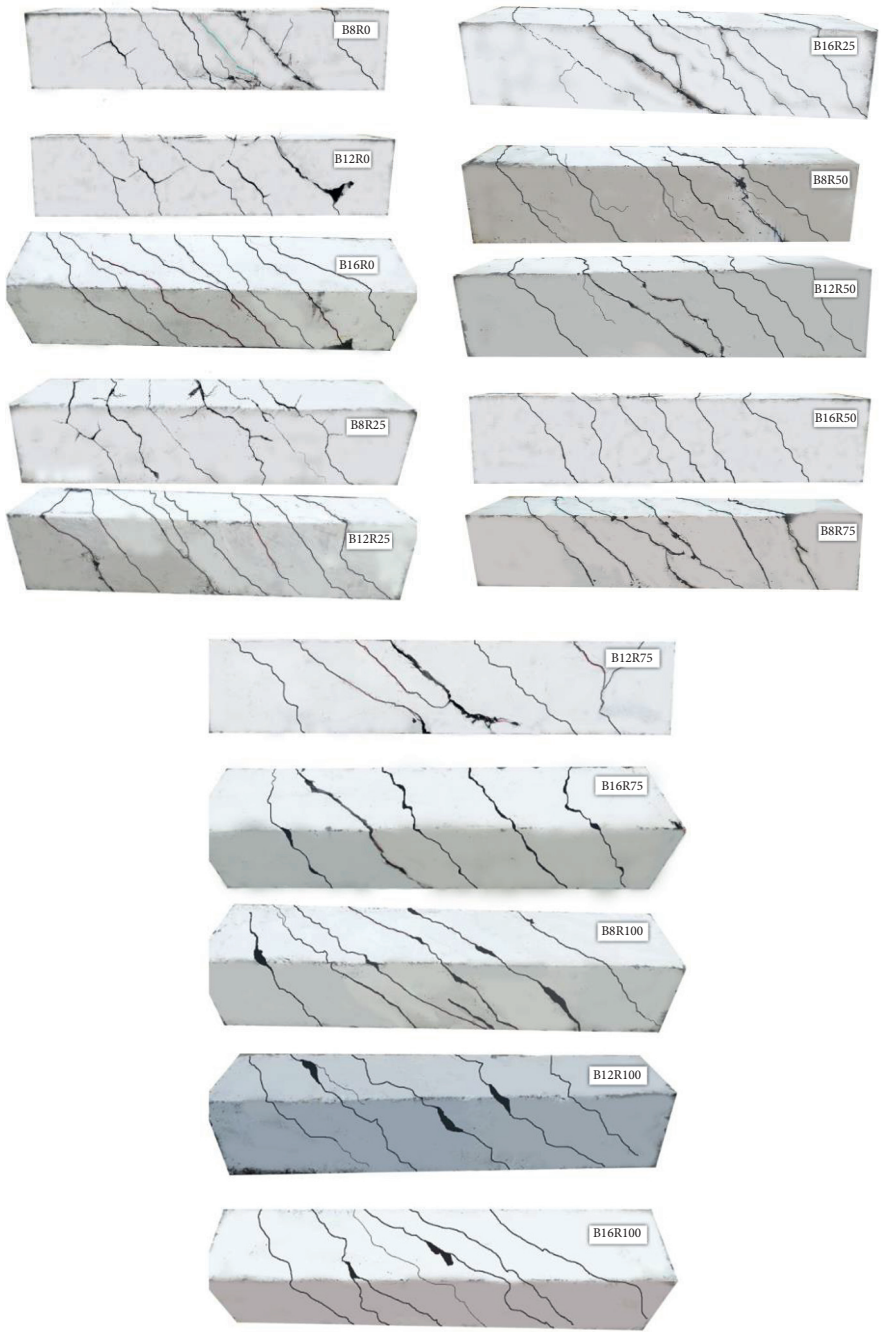

Figure 10: Crack patterns of all tested beams.

have a common behaviour in which diagonal spiral cracks appear along the beam cross-section at an angle of 450°, which is equivalent to the beam longitudinal axis. The concrete crushes in the centre of the beam as the load rises, which leads to beam collapse. There are numerous failures in the recycled concrete beams, with gaps at various angles.

5.5. Verification of the Prediction Model of Ultimate Torque. Table 4 provides that the findings of the analyses were consistent with the results of the experiments. With an average of 0.96 and identical to the ratio of oscillation, $\theta_u$test/$\theta_u$cal was modified from 0.80 to 1.12. The $\theta_u$test/$\theta_u$cal ratio grew by an average of 0.94 from 0.8 to 1.07. Table 4 provides the comparison of the experimental and theoretical predictions resulting from equation (18) for the tested beams.

In addition, the ultimate torque currently determined and the resulting torque value angles are compared with the corresponding values for flowing reinforced recycled aggregate concrete, as shown in Figure 11. The findings confirm the efficacy of the proposed system for estimating the final torque and the appropriate angle of twisting.

Table 4: Experimental and theoretical results from equation (18).

Beam	Ultimate torque (kN·m)		(T_{test}/T_{cal})	Ultimate twist (deg/m)		$(\theta_{u,test}/\theta_{u,cal})$
	$T_{u,test}$	$T_{u,cal}$		$\theta_{u,test}$	$\theta_{u,cal}$	
B8R0	110	137	0.80	2.06	1.98	1.04
B12R0	130	153	0.85	2.54	3.17	0.80
B16R0	156	179	0.87	3.65	4.01	0.91
B8R100	75	80	0.93	0.77	0.72	1.07
B12R100	97	89	1.09	0.86	0.90	0.96
B16R100	114	102	1.12	1.33	1.56	0.85

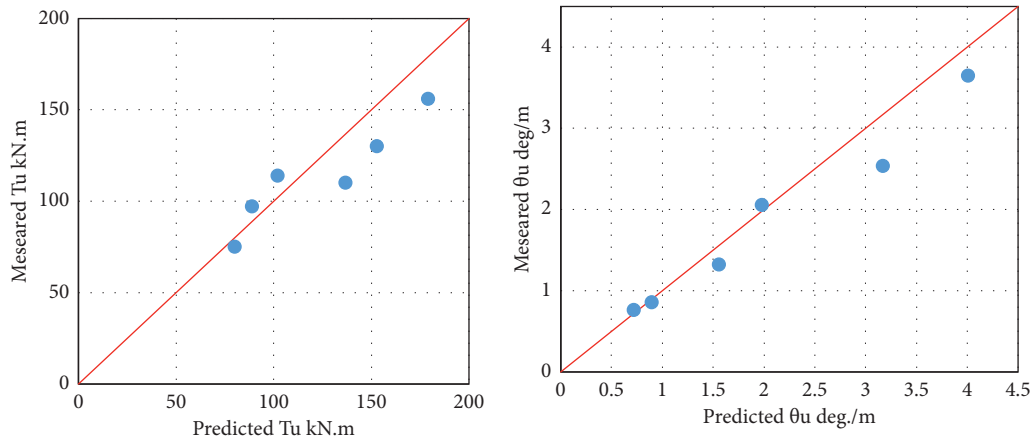

Figure 11: Measured and predicted ultimate torque and angle of twisting. (a) Measured T_u versus predicted T_u. (b) Measured θ_u versus predicted θ_u.

6. Conclusions

In this study, research was conducted to examine the impact of the torsional action of reinforced recycled concrete beams of varying recycled aggregate proportions with longitudinal steel reinforcement.

The findings show that radiators with maximum stainless steel strengthening and normally aggregated beams have maximum cracking strength and ultimate torsional strength. The presence of splitting increases, and the final strength increases as the influence of steel reinforcement is apparent in the recycling of aggregate-containing beams when recycled aggregates are used. The other aim of the analysis was to analytically predict the total reaction of torsional beams. A supported model truss was considered, and the theory predicts the torque twist reaction of the tested beams with very good accuracy.

Nomenclature

A_0: Area enclosed by the centreline of shear flow; $A_0 = A_c - (0:5)P_c t_d + t_d^2$ for a rectangular section
A_l: Total cross-sectional area of longitudinal steel bars
A_t: Cross-sectional area of one transverse steel bar
A_c: Cross-sectional area bounded by the outer perimeter of the concrete
B: Variable as defined in the constitutive relationship of mild steel embedded in concrete
$\hat{c}$: Distance from the concrete surface to the inner face of the transverse hoop bars
E_c: Elastic modulus of concrete
E_s: Elastic modulus of the steel bars
f'_c: Cylinder compressive strength of concrete
f_{cr}; ε_{cr}: Cracking stress and strain of concrete
f_l; f_t: Smeared (average) steel stress in the longitudinal and transverse directions, respectively
f_s: Smeared (average) stress of steel bars
f_y; ε_y: Yield stress and strain of bare steel bars
k_1: Ratio of the average compressive stress to the peak compressive stress in the concrete struts, neglecting the tensile stress of concrete
k_{1c}: Ratio of the average compressive stress to the peak compressive stress in the concrete struts, taking into account the tensile stress of concrete
k_{1t}: Ratio of the average tensile stress to the peak tensile stress in the concrete struts
p_0: Perimeter of the centreline of shear flow; $p_0 = p_c - 4t_d$ for rectangular sections
p_c: Perimeter of the outer concrete cross-section
p_h: Perimeter of the centre line of stirrups
q: Shear flow
Q: Variable as defined by equation (9)
R: Reduction factor for the Hsu/Zhu ratio $\nu 12$
s: Spacing of transverse hoop bars
s: In-plane displacement

t: In-plane displacement
T: Torque
T_{cr}: Cracking torque
t_d: Thickness of shear flow zone
T_u: Ultimate torque
$[T(\alpha_2)]$: Transformation matrix as defined by equation (2)
$[V]$: Conversion matrix as defined by equation (11)
$\mathscr{W}$: Out-of-plane displacement in the direction normal to the membrane element
α: Rotating angle, angle of principal compressive stress of concrete with respect to longitudinal steel bars (l-axis)
α_2: Fixed angle, angle of applied principal compressive stress (2-axis) with respect to longitudinal steel bars (l-axis)
β: Deviation angle $(\alpha_2 - \alpha)$; $2\beta = \tan^{-1}(\gamma 21/(\varepsilon 2 - \varepsilon 1))$
ε_0: Concrete cylinder strain corresponding to peak cylinder strength $f'c$
ε_1, ε_2: Smeared (average) biaxial strain in the 1-direction and 2-direction, respectively
$\overline{\varepsilon_1}$, $\overline{\varepsilon_2}$: Smeared (average) uniaxial strain in the 1-direction and 2-direction, respectively
ε_{1s}; ε_{2s}: Uniaxial surface strain in the 1-direction and 2-direction, respectively
ε_l; ε_t: Smeared (average) biaxial strain in the l-direction and the t-direction of the steel bars, respectively
$\overline{\varepsilon_l}$, $\overline{\varepsilon_t}$: Smeared (average) uniaxial strain in the l-direction and the t-direction of the steel bars, respectively
$\overline{\varepsilon_n}$: Smeared (average) uniaxial yield strain of the steel bars
$\overline{\varepsilon_s}$: Smeared (average) uniaxial strain of the steel bars
ε_{sl}: Smeared (average) strain of the steel bars that yield first, taking into account Hsu/Zhu ratios
τ_{21}: Smear (average) shear strain in the 2_1 coordinate
τ_{lt}: Smear (average) shear strain in the l_t coordinate of the steel bars
ρ: Steel ratio
$(\nu 12)$: Shear same as $\nu 12$
$(\nu 12)$: Torsion modified Hsu/Zhu ratio used in the SMMT for torsion
θ: Angle of twist per unit length
θ_{cr}: Cracking angle of twist per unit length
θ_u: Ultimate angle of twist per unit length
Ø: Curvature of the concrete struts along the 2-direction
ψ: Curvature of the concrete struts along 1-direction
ξ: Softened coefficient of concrete in compression.

Data Availability

The data used to support the findings of this study are included within the article.

Conflicts of Interest

The authors declare that they have no conflicts of interest.

References

[1] J. Chyuan-Hwan and T. T. C. Hsub, "A softened membrane model for torsion in reinforced concrete members," *Engineering Structures*, vol. 31, pp. 1944–1954, 2009.
[2] X.-N. Peng and Y.-L. Wong, "Behavior of reinforced concrete walls subjected to monotonic pure torsion-An experimental study," *Engineering Structures*, vol. 33, no. 9, pp. 2495–2508, 2011.
[3] C. E. Chalioris, "Experimental study of the torsion of reinforced concrete members," *Structural Engineering & Mechanics*, vol. 23, no. 6, pp. 713–737, 2006.
[4] C. E. Chalioris, "Tests and analysis of reinforced concrete beams under torsion retrofitted with FRP strips," *WIT Transactions on Modeling and Simulation*, vol. 46, 2007.
[5] G. Chris, "Karayannis. Smeared crack analysis for plain concrete in torsion," *Journal of Structural Engineering*, vol. 126, no. 6, 2000.
[6] C. G. Karayannis, "Experimental validation of smeared analysis for plain concrete in torsion," *Journal of Structural Engineering*, vol. 126, no. 6, 2000.
[7] J. Chyuan Hwan, "Unified softened membrane model for torsion in hollow and solid reinforced concrete members: modeling precracking and postcracking behavior," *Journal of Structural Engineering*, vol. 141, no. 10, 2015.
[8] C. E. Chalioris, "Chalioris. Behaviour model and experimental study for the torsion of reinforced concrete members," *Conference WIT Transactions on the Built Environment*, vol. 85, 2006.
[9] C. G. Karayannis and C. E. Chalioris, "Strength of prestressed concrete beams in torsion," *Structural Engineering & Mechanics*, vol. 10, no. 2, 2000.
[10] C. E. Chalioris and C. G. Karayannis, "Effectiveness of the use of steel fibres on the torsional behaviour of flanged concrete beams," *Cement and Concrete Composites*, vol. 31, no. 5, pp. 331–341, 2009.
[11] A. F. Deifalla, A. G. Zapris, and C. E. Chalioris, "Multivariable regression strength model for steel fiber," *Reinforced Concrete Beams under Torsion*, vol. 4, no. 14, 2021.
[12] I. Maruyama, M. Sogo, T. Sogabe, R. Sato, and K. Kawai, "Flexural properties of reinforced recycled concrete beams," in *Proceedings of the Internacional RILEM Conference on the Use of Recycled Materials in Buildings and Structures*, Barcelona, Spain, January 2004.
[13] B. González-Fonteboa and F. Martínez-Abella, "Shear strength of recycled concrete beams," *Construction and Building Materials*, vol. 21, no. 4, pp. 887–893, 2007.
[14] B. González-Fonteboa, F. Martínez-Abella, I. Martínez-Lage, and J. Eiras-López, "Structural shear behaviour of recycled concrete with silica fume," *Construction and Building Materials*, vol. 23, no. 11, pp. 3406–3410, 2009.
[15] H. B. Choi, C. K. Yi, H. H. Cho, and K. I. Kang, "Experimental study on the shear strength of recycled aggregate concrete beams," *Magazine of Concrete Research*, vol. 62, no. 2, pp. 103–114, 2010.
[16] G. Fathifazl, A. G. Razaqpur, O. B. Isgor, A. Abbas, B. Fournier, and S. Foo, "Flexural performance of steel-reinforced recycled concrete beams," *ACI Structural Journal*, vol. 106, no. 6, pp. 858–867, 2009.
[17] S. Sdiubert, C. Hoffmann, A. Leemann, K. Moser, and M. Motavalli, "Recycled aggregate concrete: experimental

shear resistance of slabs without shear reinforcement," *Engineering Structures*, vol. 41, pp. 490–497, 2012.
[18] J. Xiao, H. Xie, and Z. Yang, "Shear transfer across a crack in recycled aggregate concrete," *Cement and Concrete Research*, vol. 42, no. 5, pp. 700–709, 2012.
[19] G. F. Belen and M. A. Fernando, "Shear strength of recycled concrete beams," *Construction and Building Materials*, vol. 1, pp. 1–7, 2006.
[20] M. Arezoumandi and A. Smith, "An experimental study on shear strength of reinforced concrete beams with 100% recycled concrete aggregate," *Construction and Building Materials*, vol. 53, pp. 612–620, 2014.
[21] W.-C. Choi and H.-D. Yun, "Long-term deflection and flexural behavior of reinforced concrete beams with recycled aggregate," *Materials & Design*, vol. 51, pp. 742–750, 2013.
[22] G. F. Belén, M. A. Fernando, and M. L. Isabel, "Structural shear behaviour of recycled concrete with silica fume," *Construction and Building Materials*, vol. 23, pp. 3406–3410, 2009.
[23] T. T. C. Hsu and R. R. H. Zhu, "Softened membrane model for reinforced concrete elements in shear," *ACI Structural Journal*, vol. 99, no. 4, pp. 460–469, 2002.
[24] C.-H. Jeng and T. T. C. Hsu, "A softened membrane model for torsion in reinforced concrete members," *Engineering Structures*, vol. 31, no. 9, pp. 1944–1954, 2009.
[25] T. T. C. Hsu, "Shear flow zone in torsion of reinforced concrete," *Journal of Structural Engineering*, vol. 116, no. 1, Article ID 3206_26, 1990.
[26] T. T. C. Hsu, *Unified Theory of Reinforced Concrete*, CRC Press, Boca Raton, FL, USA, 1993.
[27] J. Wang, *Constitutive relationships of prestressed concrete membrane elements*, Ph.D. dissertation, University of Houston, Houston, TX, USA, 2006.
[28] M. P. Collins and D. Mitchell, "Shear and torsion design of prestressed and non-prestressed concrete beams," *PCI Journal*, vol. 25, no. 5, Article ID 32_100, 1980.
[29] T. T. C. Hsu and Y. L. Mo, "Softening of concrete in torsional members _ Theory and tests," *ACI Structural Journal*, vol. 82, no. 3, Article ID 290_303, 1985.
[30] T. T. C. Hsu and Y. L. Mo, "Softening of concrete in torsional members _ Prestressed concrete," *ACI Structural Journal*, vol. 82, no. 5, Article ID 603_15, 1985.
[31] S. A. Ashour, T. A. Samman, and T. A. Radain, "Torsional behavior of reinforced high strength concrete deep beams," *ACI Structural Journal*, vol. 96, no. 6, Article ID 1049_58, 1999.
[32] Y. L. Mo, C. H. Jeng, and Y. S. Chang, "Torsional behavior of prestressed concrete box girder bridges with corrugated steel webs," *ACI Structural Journal*, vol. 97, no. 6, Article ID 849_59, 2000.
[33] C. C. Fu and Y. Tang, "Torsional analysis for prestressed concrete multiple cell box," *Journal of Engineering Mechanics*, vol. 127, no. 1, Article ID 45_51, 2001.
[34] R. R. H. Zhu, T. T. C. Hsu, and J. Y. Lee, "Rational shear modulus for smeared crack analysis of reinforced concrete," *ACI Structural Journal*, vol. 98, no. 4, Article ID 343_50, 2001.
[35] ASTM C33/C33M-18, *Standard Specification for Concrete Aggregates*, ASTM, West Conshohocken, PA, USA, Book of Standards Volume: 04.02, 2018.
[36] ASTM C39/C39M-18, *Standard Test Method for Compressive Strength of Cylindrical Concrete Specimens*, ASTM, West Conshohocken, PA, USA, Book of Standards Volume: 04.02, 2018.
[37] ASTM C496/C496M-17, *Standard Test Method for Splitting Tensile Strength of Cylindrical Concrete Specimens*, ASTM, West Conshohocken, PA, USA, Book of Standards Volume: 04.02, 2017.